International Communications in Heat and Mass Transfer 177 (2026) 111501

Contents lists available at ScienceDirect

International Communications in Heat and Mass Transfer

journal homepage: www.elsevier.com/locate/ichmt

Coupled effects of multi-pulse laser irradiation and hyaluronic acid spacer thickness on rectal wall thermal damage during prostate cancer therapy using a GDPL bioheat model

Phanuwat Boontatao [a], Nattadon Pannucharoenwong [a,*], Phadungsak Rattanadecho [a], Piyawat sermlao [a], Suphasit Panvichien [b]

[a] Department of Mechanical Engineering, Faculty of Engineering, Thammasat School of Engineering, Thammasat University, 12120, Thailand
[b] School of Biomedical Engineering & Imaging Sciences, Faculty of Life Sciences & Medicine King's College London, WC2R 2LS, United Kingdom

ARTICLE INFO

Keywords:
Prostate cancer therapy
Multi-pulse laser irradiation
Generalized dual-phase-lag (GDPL) bioheat model
Hyaluronic acid spacer
Thermal damage

ABSTRACT

Laser-induced thermal therapy is a promising minimally invasive option for localized prostate cancer, yet excessive heat diffusion to the rectal wall remains a critical safety concern. While hyaluronic acid (HA) spacers are commonly used to mitigate rectal heating, the combined influence of spacer thickness and temporal laser modulation has not been systematically clarified. This study developed a numerical framework to investigate the coupled effects of continuous and multi-pulse laser irradiation with varying HA spacer thicknesses on rectal wall temperature and thermal damage. The generalized dual-phase-lag (GDPL) bioheat model was employed to capture non-Fourier heat transfer in biological tissue, and thermal injury was quantified using an Arrhenius damage model. Compared with continuous irradiation, multi-pulse modes markedly reduced both the peak rectal wall temperature and thermal damage. Without an HA spacer, the maximum rectal wall temperature decreased by 10.2%, 15.7%, and 20.4% for the 2-pulse, 3-pulse, and 4-pulse modes, respectively, while the corresponding thermal damage decreased by 16.9%, 25.4%, and 26.6%. The results further showed that increasing pulse number could partially compensate for reduced HA thickness. An HA spacer thickness of 3–4 mm was identified as sufficient for effective rectal wall protection. These findings provide practical guidance for improving safety and optimizing spacer usage in prostate laser therapy.

1. Introduction

Prostate cancer remains one of the most prevalent malignancies among men worldwide, with approximately 1.4 million new cases and more than 375,000 deaths reported in 2020 [1]. Although localized prostate cancer is often associated with favorable survival, treatment-related morbidity remains a major clinical concern because of the close anatomical proximity between the prostate and the anterior rectal wall [2–5]. As a result, thermal injury to adjacent healthy tissue continues to be a critical challenge in prostate cancer therapy.

Among emerging treatment modalities, laser-induced thermal therapy has gained attention as a minimally invasive option for localized prostate cancer. This technique enables localized energy deposition within tumor tissue, generating temperatures sufficient to induce coagulative necrosis while reducing invasiveness compared with conventional approaches [4,5]. However, effective treatment requires a balance between adequate tumor ablation and protection of surrounding normal tissues. In particular, excessive heat diffusion toward the rectal wall may cause complications such as rectal injury, bleeding, and long-term functional impairment [6,7]. To mitigate this risk, interstitial spacers such as hyaluronic acid (HA), polyethylene glycol (PEG), collagen, and balloon-based materials have been introduced to increase the prostate–rectum separation distance. Previous clinical and numerical studies have demonstrated that these spacers can significantly reduce rectal thermal exposure, with HA showing particularly favorable protective performance [8–10].

Reliable prediction of heat transfer in biological tissue is therefore essential for optimizing laser-based treatment protocols. The classical Pennes bioheat equation is widely used because of its simplicity, but it does not adequately represent finite-speed and non-Fourier thermal transport under rapid heating conditions such as laser irradiation [11,12]. More advanced formulations, including the dual-phase-lag

* Corresponding author.
E-mail address: pnattado@engr.tu.ac.th (N. Pannucharoenwong).

https://doi.org/10.1016/j.icheatmasstransfer.2026.111501

Available online 13 May 2026

(DPL) and generalized dual-phase-lag (GDPL) models, have been proposed to address these limitations by incorporating phase-lag effects between the heat flux and temperature gradient. Compared with the classical Pennes model, these formulations provide a more realistic description of transient thermal response in biological media exposed to short-duration or high-intensity heat sources [11–13]. In particular, the GDPL model offers greater flexibility for describing nonequilibrium thermal behavior and is therefore more suitable for the present laser-heating problem, where rapid thermal propagation and time-dependent energy delivery play important roles.

In parallel, recent studies have shown that treatment outcome is highly sensitive to controllable parameters such as laser power, exposure time, and energy-delivery strategy [14]. While most previous spacer-assisted prostate laser studies have focused on continuous irradiation or fixed delivery conditions [9,10], pulsed and repeated-pulse laser modes have been reported to alter heat accumulation, coagulation behavior, and thermal damage evolution [15–17]. These findings suggest that temporal laser modulation may serve as an additional control parameter for improving treatment safety. Nevertheless, the coupled effects of laser irradiation mode and HA spacer thickness on rectal wall thermal protection have not yet been systematically examined within a multilayer prostate model using an advanced non-Fourier bioheat formulation.

Therefore, the present study numerically investigates the combined effects of continuous and multi-pulse laser irradiation and HA spacer thickness on temperature distribution and thermal damage during prostate cancer treatment. A two-dimensional multilayer biological model consisting of the rectal wall, HA spacer, the fat layer, prostate, and tumor is developed. The GDPL bioheat formulation is employed to capture transient non-Fourier heat transfer, and thermal injury is evaluated using an Arrhenius damage model. The specific objectives are to examine (i) the influence of pulse number and temporal energy delivery on rectal wall heating, (ii) the effect of HA spacer thickness on thermal protection, and (iii) the resulting thermal damage in both tumor and rectal wall regions. The findings of this study are expected to provide practical guidance for optimizing laser-delivery protocols and spacer design to improve both treatment safety and therapeutic effectiveness in prostate cancer therapy.

2. Mathematical formulation

2.1. Governing equations

To describe laser-induced heat transfer in vascularized biological tissue, a local thermal non-equilibrium (LTNE) formulation was adopted. In this framework, blood and tissue are treated as two interacting phases with distinct local temperatures, denoted by T_b and T_t respectively. This approach is more suitable than the classical Pennes model for the present problem because it explicitly accounts for thermal interaction between blood and tissue and provides a foundation for incorporating non-Fourier heat transfer behavior under rapid laser heating conditions. The transient energy equations governing the blood and tissue phases can be written as follows [13,16,18].

Blood Phase:

$$\varepsilon(\rho c)_b\left(\frac{\partial T_b}{\partial t}+V\bullet\nabla T_b\right)=\varepsilon k_b\left(\nabla^2 T_b+a_h h_b(T_t-T_b)+w\rho_b c_b(T_t-T_b)\right.$$

$$\left.+\varepsilon Q_{mb}+\varepsilon Q_{laser}\right. \tag{1}$$

Tissue Phase:

$$(1-\varepsilon)(\rho c)_t\frac{\partial T_t}{\partial t}=(1-\varepsilon)k_t\left(\nabla^2 T_t\right)-a_h h_b(T_t-T_b)-w\rho_b c_b(T_t-T_b)$$

$$+(1-\varepsilon)Q_{mt}+(1-\varepsilon)Q_{laser} \tag{2}$$

The interfacial heat exchange between blood and tissue is represented by a lumped coupling coefficient, defined as

$$G=a_h h_b+wc_b \tag{3}$$

where a_h denotes the capillary surface area per unit tissue volume, h_b is the convective heat transfer coefficient at the blood–tissue interface, and w is the blood perfusion rate. Here, ε is the issue porosity, while Q_{mb}, Q_{mt} and Q_{laser} denote the metabolic heat generation in the blood phase, the metabolic heat generation in the tissue phase, and the laser heat source, respectively. Under LTNE conditions, the transient thermal interaction between the two phases can be written as [17–19].

$$\varepsilon(\rho c)_b\frac{\partial T_b}{\partial t}=G(T_t-T_b) \tag{4}$$

Rearranging Eq. (4) gives the following relationship between the tissue and blood temperatures:

$$T_t=T_b+\frac{\varepsilon\rho_b C_b}{(a_h h_b+wc_b)}\frac{\partial T_b}{\partial t}=T_b+\frac{\varepsilon\rho_b C_b}{\mathrm{G}}\frac{\partial T_b}{\partial t} \tag{5}$$

By combining Eqs. (1) and (2), a modified expression under LTNE conditions is first obtained as

$$\varepsilon(\rho c)_b\frac{\partial T_b}{\partial t}+(1-\varepsilon)(\rho c)_t\frac{\partial T_t}{\partial t}+\varepsilon(\rho c)_b(V\bullet\nabla T_b)$$
$$=\varepsilon k_b\left(\nabla^2 T_b\right)+(1-\varepsilon)k_t\left(\nabla^2 T_t\right)$$

$$+(1-\varepsilon)Q_{mt}+\varepsilon Q_{mb}+Q_{laser} \tag{6}$$

Substituting Eq. (5) into Eq. (6) and rearranging the resulting terms yields the following reduced dual-phase-lag-type formulation in terms of the blood temperature:

$$\frac{\partial T_b}{\partial t}+\tau_q\frac{\partial^2 T_b}{\partial t^2}+\frac{\varepsilon(\rho c)_b}{(\rho C)_{eff}}(V\bullet\nabla T_b)=\alpha_{eff}\left(\nabla^2 T_b+\tau_t\frac{\partial}{\partial t}\left(\nabla^2 T_b\right)\right)$$

$$+\frac{\varepsilon Q_{mb}+(1-\varepsilon)Q_{mt}+Q_{laser}}{(\rho C)_{eff}} \tag{7}$$

For convenience, the effective thermophysical properties used in Eq. (7) are defined as follows [11,16]:

$$(\rho C)_{eff}=\varepsilon\rho_b C_b+(1-\varepsilon)\rho_t C_t \tag{8}$$

$$k_{eff}=\varepsilon k_b+(1-\varepsilon)k_t \tag{9}$$

$$\alpha_{eff}=\frac{k_{eff}}{(\rho C)_{eff}} \tag{10}$$

where $(\rho C)_{eff}$, k_{eff} and α_{eff} denote the effective volumetric heat capacity, effective thermal conductivity and effective thermal diffusivity, respectively. The phase-lag times associated with the heat flux and temperature gradient are given by

$$\tau_t=\frac{\varepsilon\,(1-\varepsilon)}{\left[\frac{\varepsilon}{k_{tb}}+(1-\varepsilon)\right]}\frac{\rho_b C_b}{G} \tag{11}$$

$$\tau_q=\frac{\varepsilon\,(1-\varepsilon)}{\left[\frac{\varepsilon}{C_{tb}}+(1-\varepsilon)\right]}\frac{\rho_b C_b}{G} \tag{12}$$

where $C_{tb}=C_t/C_b$ and $k_{tb}=k_t/k_b$ Here, τ_t denotes the phase-lag time associated with the delayed establishment of the temperature gradient, whereas τ_q represents the phase-lag time associated with the delayed response of the heat flux. These lag times arise from the thermal nonequilibrium between blood and tissue and reflect the finite-speed nature of thermal propagation in vascularized biological media. Physically, they characterize the temporal mismatch between local energy deposition and the subsequent thermal response, which becomes

particularly important under rapid and transient heating conditions such as laser irradiation. Therefore, the inclusion of τ_t and τ_q enables the model to capture non-Fourier thermal behavior more realistically than the classical Pennes formulation [11].

Using the effective thermophysical properties and phase-lag parameters defined above, the generalized dual-phase-lag (GDPL) bioheat equation employed in the present study can be written in terms of the tissue temperature as

$$\frac{\partial T_t}{\partial t}+\tau_q\frac{\partial^2 T_t}{\partial t^2}-\frac{G}{(\rho C)_{eff}}(T_b-T_t)=\alpha_{eff}\left(\nabla^2 T_t+\tau_t\frac{\partial}{\partial t}(\nabla^2 T_t)\right)$$

$$+\frac{\varepsilon Q_{mb}+(1-\varepsilon)Q_{mt}+Q_{laser}}{(\rho C)_{eff}}$$

$$+\frac{\varepsilon(\rho c)_b}{G(\rho C)_{eff}}\left(\varepsilon\frac{\varepsilon Q_{mb}}{\partial t}+(1-\varepsilon)\frac{\partial Q_{mt}}{\partial t}+\frac{\partial Q_{laser}}{\partial t}\right) \quad (13)$$

In deriving Eq. (13), the temporal variation of blood velocity was neglected, i.e. $\partial V/\partial t \approx 0$, and the convective contribution was approximated through the interphase heat exchange relation under LTNE conditions [11,16]. Eq. (13) was employed as the governing bioheat equation in the prostate and tumor domains throughout the present simulations.

2.2. Laser heat source model

The volumetric heat source generated by laser irradiation was modeled using the Beer–Lambert law combined with a Gaussian radial beam distribution. This formulation accounts for both the exponential attenuation of laser intensity along the penetration depth and the non-uniform spatial distribution of energy around the laser axis [20–22]. Accordingly, the absorbed laser energy within the tissue domain can be written as

$$Q_{laser}(r,z,t)=Q_0(r,z)S(t) \quad (14)$$

where Q_{laser} denotes the volumetric heat generation term (W/m^3), r and z are the radial and axial coordinates, respectively, $Q_0(r,z)$ is the spatially distributed laser heat source and $S(t)$ is the temporal modulation function representing the irradiation pattern. Assuming a Gaussian beam profile at the tissue surface, the spatial laser source term is expressed as [14,23].

$$Q_0(r,z)=\alpha_{eff}\frac{P}{2\pi\sigma^2}exp\left(-\frac{r^2}{2\sigma^2}\right)\exp(-\alpha_{eff}Z) \quad (15)$$

where P is the laser power and σ is the standard deviation associated with the beam radius. In the present study, σ was related to the optical fiber radius r_f through $\sigma=\frac{r_f}{3}$. The effective attenuation coefficient was used to incorporate both absorption and scattering effects in biological tissue and was evaluated as

$$\alpha_{eff}=\sqrt{3\alpha(\alpha+\alpha_s(1-g))} \quad (16)$$

where α is the absorption coefficient, α_s is the scattering coefficient, and g is the anisotropy factor. This expression enables the laser source term to reflect the combined influence of optical absorption and forward scattering during photon transport in tissue.

To distinguish between continuous and multi-pulse irradiation, a temporal modulation function $S(t)$ was introduced. For generality, it is defined using the Heaviside step function $H(\cdot)$ as [16,17,20]

$$S(t)=\sum_{n=1}^{N}\left[H\left(t-t_n^{on}\right)-H\left(t-t_n^{off}\right)\right] \quad (17)$$

where N is the number of pulses, while t_n^{on} and t_n^{off} are the starting and ending times of the n-th irradiation interval, respectively. This formulation allows a unified representation of continuous, 2-pulse, 3-pulse, and 4-pulse laser delivery modes. The corresponding temporal irradiation profiles are illustrated in Fig. 1, and the irradiation scenarios are summarized in Table 1. To ensure a fair basis for comparison, the laser power was fixed at 3 W, the total laser-on time was maintained at 300 s, and the total simulation time was set to 600 s for all cases. Thus, the selected ON/OFF intervals yield identical total delivered energy, and the differences among cases arise solely from the temporal partitioning of that energy. This design enables the isolated effect of temporal laser modulation on rectal wall protection and tumor ablation performance to be systematically evaluated.

2.3. Geometry and boundary conditions

A two-dimensional axisymmetric domain was constructed to simulate laser-induced heat transfer in a prostate tumor adjacent to the rectal wall with hyaluronic acid (HA) spacer protection, as shown in Fig. 2. The model comprises five subregions the rectal wall, HA spacer, the fat layer, prostate gland, and tumor. The rectal wall thickness was fixed at L_1 = 2.6 mm, the fat layer thickness at L_2 = 4 mm, and the prostate thickness at L_3 = 40 mm. The HA spacer thickness, d_x, was varied as 0, 2, 3, 4, and 5 mm. A tumor with a diameter of 10 mm was positioned within the prostate near the laser heating zone [9].

The boundary and initial conditions employed in this study are depicted in Fig. 3. The axisymmetric r-z formulation was adopted to represent the radial spread and axial penetration of heat while reducing computational cost. Initially, the entire domain was assumed to be at the physiological temperature.

$$T(r,z,0)=37^{\circ}C \quad (18)$$

A convective boundary condition was imposed at the outer surface of the rectal wall,

$$-k\nabla T\cdot n=h(T-T_\infty) \quad (19)$$

with $T_\infty=37^{\circ}C$ The symmetry axis satisfied.

$$\frac{\partial T}{\partial r}=0 \quad (20)$$

whereas the remaining external boundaries were assumed adiabatic.

$$-k\nabla T\cdot n=0 \quad (21)$$

$$T_u=T_d \quad (22)$$

$$-k_u\nabla T_u\cdot n=-k_d\nabla T_d\cdot n \quad (23)$$

These conditions ensure physically consistent heat transfer across the multilayer prostate-rectum system. Laser heating was modeled as a Gaussian volumetric source with depth-dependent attenuation, enabling simulation of both continuous and multi-pulse irradiation conditions.

2.4. Thermal damage model

Irreversible thermal injury may occur when biological tissue is exposed to elevated temperatures for a sufficient duration. In thermal therapy, accurate estimation of both temperature level and exposure time is therefore essential, particularly to ensure effective tumor destruction while preventing unintended damage in surrounding healthy tissues. In the present study, thermal damage was quantified using the Arrhenius model, which relates tissue injury to a temperature-dependent chemical reaction rate and has been widely applied in laser ablation and bioheat-transfer studies [13,15,16]. The damage integral is expressed as

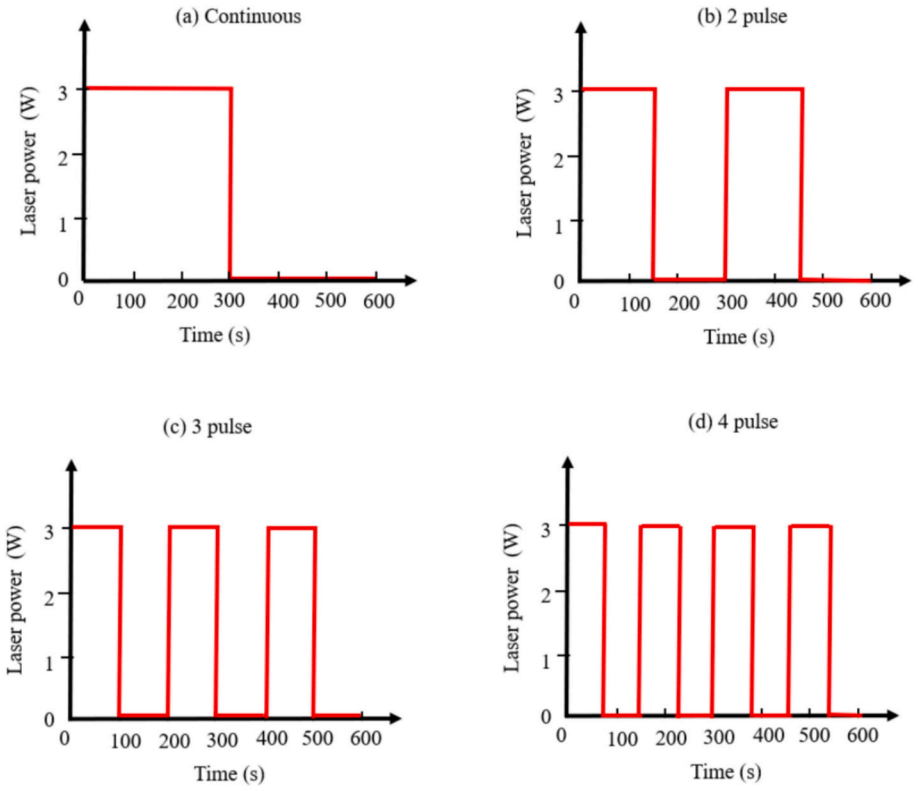

Fig. 1. Temporal profiles of laser irradiation modes considered in the present study: (a) continuous, (b) 2-pulse, (c) 3-pulse, and (d) 4-pulse. In all cases, the laser power was fixed at 3 W, the total laser-on time was maintained at 300 s, and the total simulation time was 600 s.

Table 1
Summary of continuous and multi-pulse laser irradiation scenarios used in the simulations.

Case	Number of pulses	ON intervals (s)	Total laser-on time (s)	Total simulation time (s)
Continuous	1	0–300	300	600
2-pulse	2	0–150, 300–450	300	600
3-pulse	3	0–100, 200–300, 400–500	300	600
4-pulse	4	0–75, 150–225, 300–375, 450–525	300	600

$$\Omega = \int_0^t A e^{\left(-\frac{E_a}{R(T_t+273)}\right)} dt \tag{24}$$

where Ω is the dimensionless thermal damage parameter, A is the frequency factor (s^{-1}), E_a is the activation energy (J/mol), R is the universal gas constant (J/(mol·K)) and (T_t + 273) is the local tissue temperature (K). The Arrhenius formulation relates cumulative thermal exposure to the degree of irreversible protein denaturation and cellular destruction. In general, tissue temperatures above approximately 55–60 °C may initiate irreversible thermal injury if maintained for a sufficient duration. Within the Arrhenius framework, Ω represents the cumulative extent of thermally induced tissue damage. A value of $\Omega = 1$ is commonly interpreted as the onset of irreversible thermal injury, whereas $\Omega < 1$ and $\Omega > 1$ correspond to sub-threshold and more severe irreversible damage, respectively [16,17]. In the present study Eq. (24) was applied to both the tumor and rectal wall regions in order to assess treatment effectiveness and collateral thermal injury simultaneously. In this way, the Arrhenius model provides a quantitative measure linking the transient temperature field predicted by the GDPL bioheat model to biologically meaningful tissue response.

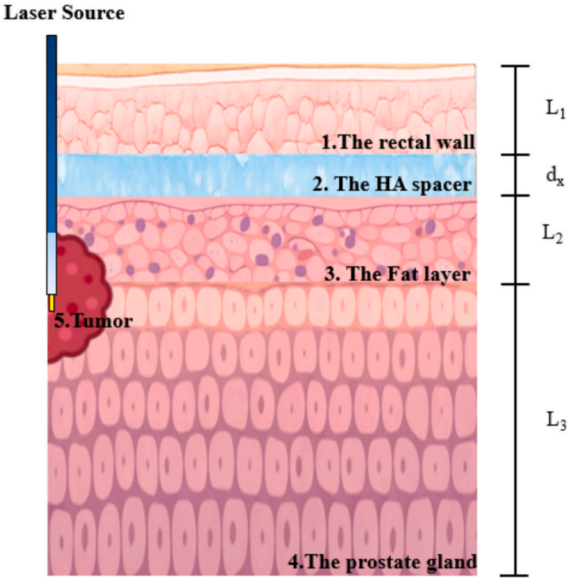

Fig. 2. Multilayer geometry of the prostate tissue model used in the simulations.

2.5. *Thermophysical properties used in the simulations*

The thermophysical properties assigned to the computational domains are summarized in Table 2. The present model includes the prostate tissue, tumor tissue, rectal wall, the fat layer, and the

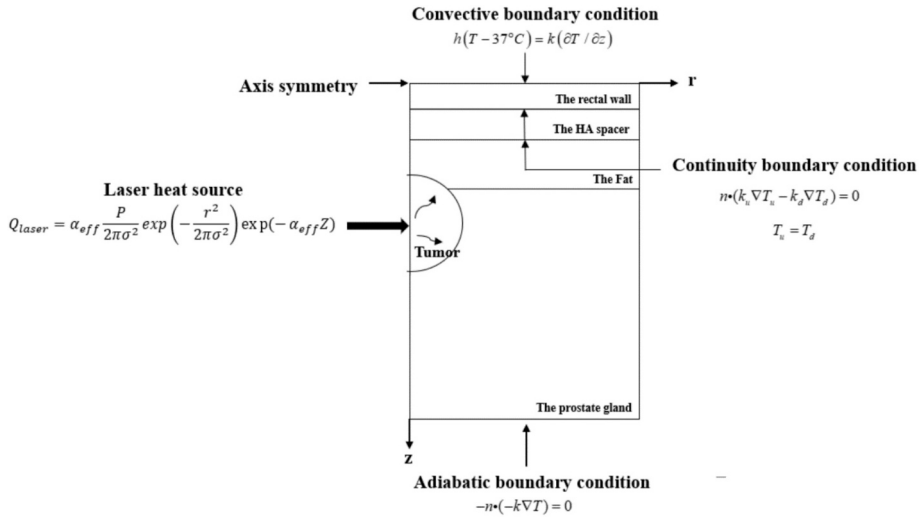

Fig. 3. Schematic of the computational domain and applied boundary conditions for the axisymmetric multilayer prostate model.

Table 2
Thermophysical and optical properties of biological tissues, blood, and HA spacer used in the simulations [9,10,18,23].

Material/ Region	Prostate	Tumor	Blood	The fat layer	Rectal wall	HA spacer
$\rho\left(\frac{kg}{m^3}\right)$	1079	1079	1000	1009	1027	1800
$C_l\left(\frac{J}{kg.K}\right)$ $T<100^\circ C$	4000	4000	4180	2713	2372	2233
$C_{p_g}\left(\frac{J}{kg.K}\right)$ $T>100^\circ C$	2156	2156	2156	2713	2372	2233
$k\left(\frac{W}{m.k}\right)$	0.52	0.52	0.51	0.36	0.39	0.272
$w_b\left(\frac{1}{s}\right)$	5.6×10^{-3}	5.6×10^{-3}	–	5×10^{-4}	5×10^{-4}	–
ε	0.28	0.28	–	0.1	0.1	–
$\alpha\left(\frac{1}{m}\right)$	α_h 30 α_c 40	–	–	–	–	–
$\alpha_s\left(\frac{1}{m}\right)$	$\alpha_{s,h}$8000 $\alpha_{s,c}$18,000	–	–	–	–	–
g	0.95					

hyaluronic acid (HA) spacer, together with the blood-related properties required in the perfusion terms of the bioheat formulation. The selected parameters include density ρ, specific heat capacity c, thermal conductivity k, blood perfusion rate w_b, porosity ε, absorption coefficient α, scattering coefficient α_s, and anisotropy factor g, depending on the role of each region in the thermal and optical modeling. In addition, $\alpha_h$and α_c denote the absorption coefficients of healthy and coagulated tissues, respectively, whereas $\alpha_{s,h}$ and $\alpha_{s,c}$ represent the corresponding scattering coefficients. These optical parameters were used to determine the effective attenuation coefficient in the laser heat source model.

Because localized temperatures may exceed $100^\circ C$ under intense laser exposure, particularly for small spacer thicknesses or continuous irradiation, the thermal response in the high-temperature regime was represented using an effective heat-capacity treatment. For temperatures below $100^\circ C$, the conventional heat capacity C_l was used. For temperatures above $100^\circ C$, an effective high-temperature heat capacity C_{p_g} was prescribed to account for the additional energy associated with tissue dehydration and water vaporization. This treatment improves the physical realism of the simulations in cases where strong localized heating occurs [14,23,24].

Among the modeled regions, the HA spacer plays a key role in limiting heat propagation from the laser-heated prostate and tumor regions toward the rectal wall because of its relatively low thermal conductivity. Therefore, the thermophysical contrast between the biological tissues and the HA layer directly influences rectal thermal protection. The properties listed in Table 2 were used consistently in all simulated cases to evaluate the coupled effects of irradiation mode and HA spacer thickness on temperature elevation and thermal damage.

3. Methodology

A numerical framework was established to investigate the effects of continuous and multi-pulse laser irradiation on heat transfer and thermal damage during prostate laser therapy with hyaluronic acid (HA) spacer protection. The analysis focused on the coupled effects of temporal energy delivery and spacer thickness on tumor ablation efficacy and rectal wall safety. The simulations were performed using the finite element method in COMSOL Multiphysics. A two-dimensional axisymmetric multilayer model was employed, consisting of the rectal wall, HA spacer, the fat layer, prostate gland, and tumor. The thicknesses of the rectal wall, the fat layer, and prostate were fixed at 2.6, 4, and 40 mm, respectively, whereas the tumor diameter was fixed at 10 mm. The HA spacer thickness was varied as 0, 2, 3, 4, and 5 mm [25].

The thermophysical and optical properties of each domain were assigned according to values reported in the literature. Laser heating was represented by a Gaussian volumetric heat source with a power of 3 W. The total simulation time was set to 600 s, while the total laser-on time was fixed at 300 s for all irradiation modes. Four irradiation scenarios were examined: continuous, 2-pulse, 3-pulse, and 4-pulse modes. The transient temperature distribution was calculated using the generalized dual-phase-lag (GDPL) bioheat model, while thermal damage was evaluated through the Arrhenius damage integral. For each case, the temperature history and thermal damage evolution were analyzed in both the tumor and rectal wall regions.

A mesh independence study was performed to ensure the numerical accuracy and convergence of the simulation results. As shown in Fig. 4, the predicted temperature varied noticeably at coarse mesh densities but gradually converged as the number of elements increased. Beyond approximately 40,000 elements, further mesh refinement produced only negligible changes in the temperature prediction. Therefore, a mesh containing about 60,000 elements was selected as an optimal compromise between computational efficiency and solution accuracy.

The overall computational workflow is illustrated in Fig. 5. This methodology provides a systematic basis for assessing whether multi-pulse irradiation can reduce rectal thermal injury without

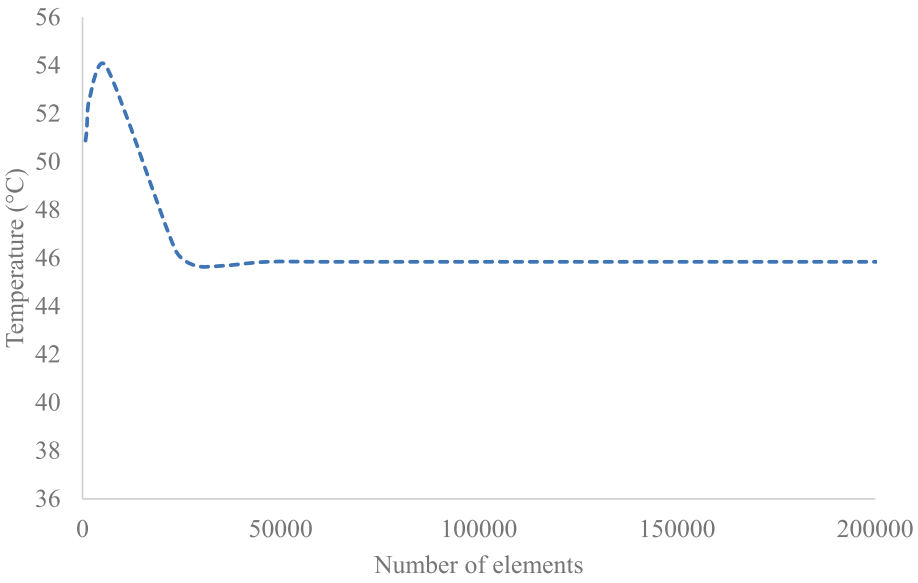

Fig. 4. Mesh independence study showing convergence with increasing element numbers.

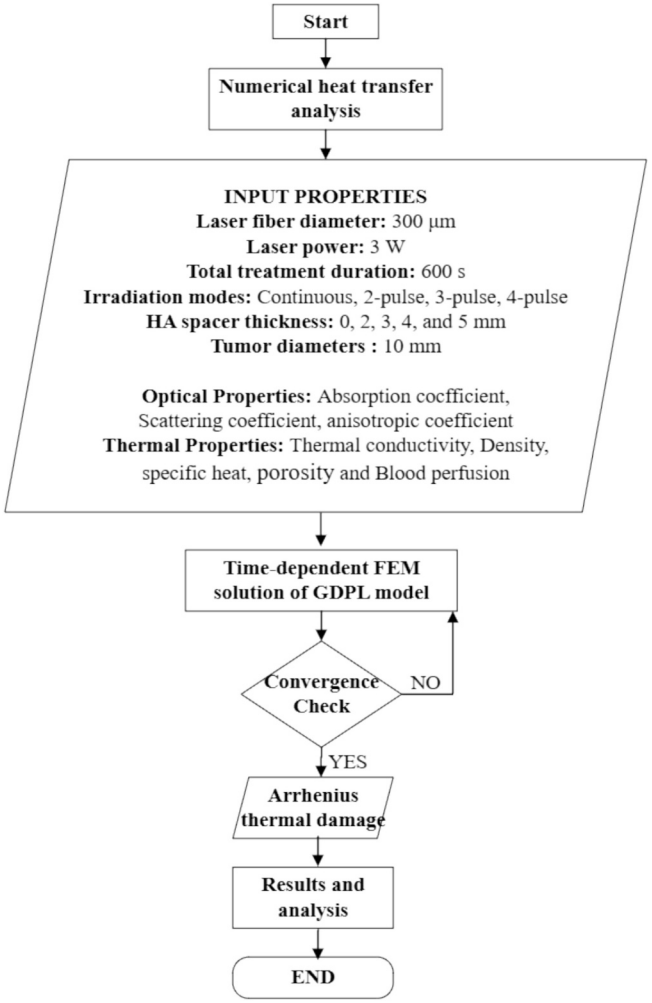

Fig. 5. Schematic workflow of the numerical methodology for assessing rectal thermal injury reduction and tumor ablation performance during multi-pulse prostate laser therapy.

compromising tumor ablation performance.

4. Results and discussion

The numerical results are presented and discussed in this section to clarify the coupled effects of laser irradiation mode and HA spacer thickness on rectal wall thermal protection during prostate laser therapy. The analysis is based on the GDPL bioheat model, which is used to predict the temperature response and Arrhenius-based thermal damage in both the rectal wall and tumor regions under continuous and multi-pulse irradiation conditions. Particular attention is given to the roles of temporal energy modulation and spacer-assisted separation in reducing collateral thermal injury while maintaining effective tumor ablation. The reliability of the model is first examined through validation against published data, followed by a systematic discussion of the resulting thermal behavior and treatment implications.

4.1. Model validation

To assess the reliability of the present numerical model, the predicted transient rectal wall temperature was validated against the published results of Namakshenas and Mojra for focal laser ablation of a prostate peripheral zone tumor without a PEG-based hydrogel spacer. For consistency with the reference study, the HA spacer thickness in the present validation was set to 0 mm, and the boundary conditions were matched to those reported in the benchmark case. The validation was performed under identical operating conditions, with a laser power of 4 W and irradiation durations of 5, 10, and 20 s, consistent with the benchmark case reported in the reference study. As illustrated in Fig. 6 the temperature histories predicted by the present model closely match the published results for all three irradiation durations. In each case, the model accurately reproduces the rapid rise in rectal wall temperature during laser irradiation, followed by a gradual cooling phase after laser shutoff. The agreement is particularly strong in terms of peak temperature, time to peak, and the subsequent cooling behavior.

4.2. Transient temperature evolution in the rectal wall without HA spacer

Fig. 7 presents the transient temperature histories of the rectal wall under continuous and multi-pulse laser irradiation in the absence of HA spacer protection. A clear difference in thermal response is observed among the irradiation modes, indicating that temporal energy delivery strongly influences heat accumulation within the rectal wall. Under continuous irradiation, the rectal wall temperature increases

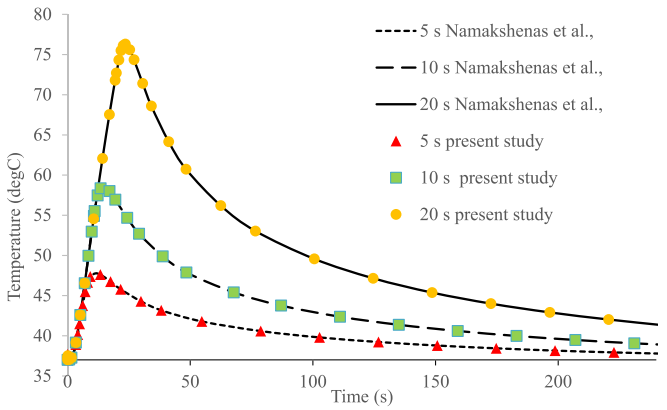

Fig. 6. Comparison of the predicted rectal wall temperature histories with the published results of Namakshenas and Mojra [9] for validation of the present model.

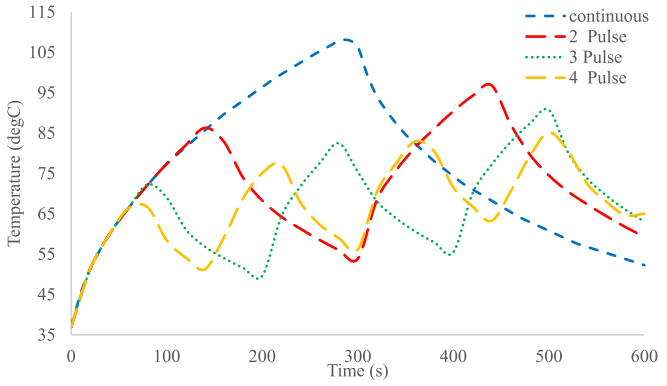

Fig. 7. Comparison of transient rectal wall temperature histories under continuous, 2-pulse, 3-pulse, and 4-pulse laser irradiation in the absence of HA spacer protection.

monotonically during the laser-on period and reaches the highest peak among all investigated cases. This behavior occurs because laser energy is delivered continuously, allowing heat to accumulate progressively within the tissue with limited opportunity for dissipation during exposure. As a result, conductive heat transfer from the laser-heated prostate and tumor regions toward the rectal wall proceeds without interruption, leading to pronounced thermal buildup and the largest temperature rise. After the laser is turned off, the rectal wall temperature gradually decreases; however, the overall thermal load remains substantially higher than that observed in the pulsed cases.

In contrast, the multi-pulse modes exhibit a distinctly oscillatory temperature profile, reflecting repeated heating and cooling cycles during the ON and OFF intervals. During each ON period, the rectal wall temperature rises due to laser-induced heating and subsequent thermal conduction through the intervening tissue layers. During each OFF period, partial cooling takes place, which interrupts continuous heat accumulation and reduces the peak temperature attained in the rectal wall. Consequently, the maximum rectal wall temperature decreases as the number of pulses increases. Among the pulsed conditions, the 4-pulse mode produces the lowest temperature peaks, followed by the 3-pulse and 2-pulse modes. From a physical perspective, this behavior is governed by the competition between energy deposition and thermal diffusion. Although the total laser-on time is identical in all cases, redistribution of the same total energy into shorter irradiation intervals introduces cooling windows that allow part of the stored heat to dissipate before the subsequent pulse begins. This suppresses cumulative heat buildup and lowers the peak rectal wall temperature. Similar trends have been reported in previous studies on pulsed or repetitive laser irradiation, where intermittent energy delivery was shown to reduce thermal accumulation and mitigate collateral heating compared with continuous exposure [16].

These results demonstrate that pulse modulation alone can significantly alleviate rectal thermal loading even without spacer protection. This finding suggests that temporal control of laser delivery can serve as an effective strategy for improving treatment safety, particularly in situations where no protective spacer is used or where spacer thickness is limited. The observed reduction in peak rectal temperature with increasing pulse number is also consistent with the general thermal advantage of intermittent laser delivery reported in the literature.

4.3. *Effect of a 4 mm HA spacer on rectal wall temperature*

Fig. 8 compares the transient rectal wall temperature histories under continuous and multi-pulse laser irradiation when a 4 mm hyaluronic acid (HA) spacer is positioned between the prostate and the rectal wall. Compared with the no-spacer condition, the rectal wall temperature is markedly reduced for all irradiation modes, confirming the strong thermal protective effect of the HA layer. This reduction is primarily attributed to two mechanisms: the increased separation distance between the laser-heated prostate region and the rectal wall, and the relatively low thermal conductivity of the HA spacer, both of which suppress conductive heat transfer toward the rectum. Under continuous irradiation, the rectal wall still reaches the highest temperature among the four irradiation modes. However, the peak temperature is substantially lower than that observed in the absence of the spacer, indicating that a 4 mm HA layer can effectively attenuate thermal propagation even under the most thermally aggressive delivery mode. In the multi-pulse cases, the rectal wall temperature rises more gradually and remains within a narrower range throughout the treatment period. Relative to the no-spacer condition, the oscillatory behavior becomes less pronounced, particularly for the 3-pulse and 4-pulse modes.

From a physical standpoint, this smoother thermal response arises from the combined action of spatial insulation and temporal modulation. The HA spacer reduces the magnitude of heat conducted to the rectal wall, while the OFF intervals between pulses allow partial cooling before the onset of the subsequent heating cycle. Consequently, thermal accumulation is further suppressed, leading to a more stable rectal wall temperature history and a lower maximum temperature. Similar thermal benefits of intermittent or repetitive pulse delivery, compared with continuous irradiation, have been reported in previous studies on laser heating in biological tissues [20]. An important observation is that, once a 4 mm HA spacer is introduced, the temperature differences among the irradiation modes become much smaller than those observed without

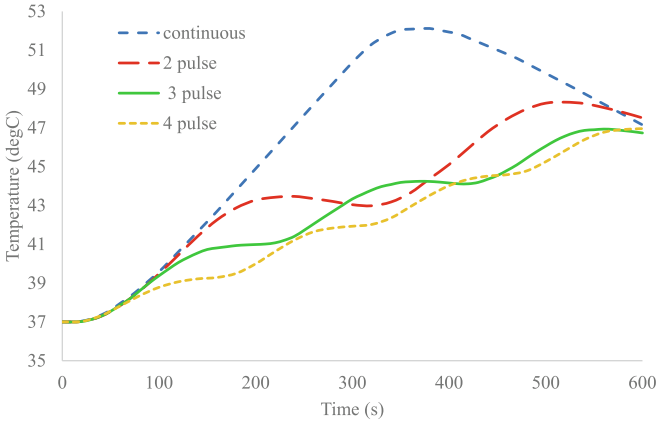

Fig. 8. Comparison of transient rectal wall temperature histories under continuous, 2-pulse, 3-pulse, and 4-pulse laser irradiation in the presence of a 4 mm HA spacer.

spacer protection. This suggests that, at this thickness, the dominant protective mechanism is the spatial thermal shielding provided by the spacer, whereas pulse modulation offers an additional but comparatively smaller benefit. Nevertheless, the pulsed modes still maintain lower rectal wall temperatures than continuous irradiation, indicating that multi-pulse delivery remains advantageous even in the presence of a clinically relevant spacer thickness. Overall, these results show that combining a 4 mm HA spacer with pulse-modulated laser delivery improves rectal thermal safety more effectively than either strategy alone.

4.4. Thermal damage evolution in tumor and rectal wall

Fig. 9 shows the temporal evolution of thermal damage in the tumor for continuous and multi-pulse laser irradiation. In all irradiation modes, the Arrhenius damage parameter increases rapidly during the early stage of treatment and approaches the threshold associated with effective thermal destruction of tumor tissue. Continuous irradiation reaches this level earliest, followed closely by the 2-pulse mode, whereas the 3-pulse and 4-pulse modes exhibit a slightly slower accumulation rate. Nevertheless, all cases ultimately approach a damage level close to $\Omega \approx 1$, which is commonly regarded as the onset of irreversible tissue injury and therefore a practical indicator of effective thermal ablation. In the present study, this criterion was interpreted together with the corresponding tumor temperature history rather than in isolation. Since the tumor region reached the therapeutic coagulation range while the predicted damage parameter approached $\Omega \approx 1$, the results indicate that effective tumor ablation can still be achieved even when the same total laser-on time is redistributed into multiple pulses. From a physical standpoint, this behavior reflects the fact that the tumor is located closest to the laser heat source and therefore experiences the highest local energy deposition. Consequently, although short cooling intervals slightly reduce the transient rate of damage accumulation, the cumulative thermal dose remains sufficient to sustain irreversible protein denaturation and cellular injury. Therefore, the multi-pulse strategy reduces excessive heating in surrounding tissue while preserving effective tumor ablation.

In contrast, the rectal wall exhibits much greater sensitivity to irradiation mode because it is separated from the heated tumor region and receives thermal energy mainly through conduction across the intervening tissue layers. As shown in Fig. 10, when no HA spacer is used, continuous irradiation produces the most severe thermal damage in the rectal wall, with Ω increasing steadily throughout the heating period and remaining markedly higher than in the pulsed cases. The 2-pulse, 3-pulse, and 4-pulse modes all reduce rectal wall damage substantially, and the magnitude of reduction becomes greater as the number of pulses increases. This trend is physically consistent with interrupted energy delivery: each OFF interval allows partial cooling and reduces cumulative heat build-up before the next pulse begins. As a result, the rectal

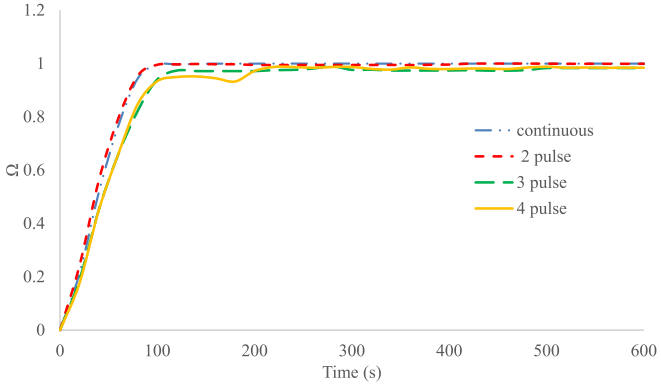

Fig. 9. Temporal evolution of thermal damage in the tumor under continuous and multi-pulse laser irradiation.

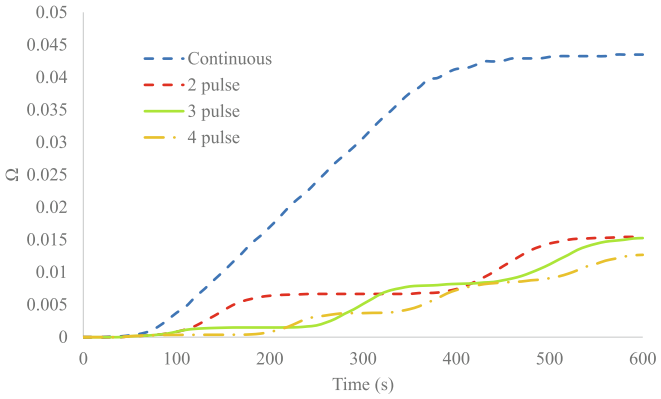

Fig. 10. Rectal wall thermal damage histories without HA spacer under continuous and multi-pulse irradiation.

wall experiences a lower effective thermal dose even though the total laser-on time remains unchanged. Previous studies on multiple-pulse and repetitive laser heating likewise reported that intermittent irradiation can mitigate collateral thermal damage relative to continuous exposure. [16,17]

The protective effect becomes even more evident when a 4 mm HA spacer is introduced, as shown in Fig. 11. Under this condition, rectal wall thermal damage is dramatically suppressed in all irradiation modes, and the corresponding Ω values remain substantially lower than those obtained without spacer protection. Continuous irradiation still yields the highest damage among the four modes, but its level is greatly reduced compared with the no-spacer case. The pulsed modes further suppress damage, with the 4-pulse condition producing the lowest rectal wall injury. This pronounced reduction is attributed to the combined effects of spatial and temporal protection. Spatially, the HA spacer increases the prostate–rectum separation and acts as a low-conductivity thermal barrier, thereby weakening conductive heat transfer toward the rectal wall. Temporally, pulse interruption introduces cooling intervals that further limit thermal accumulation.

An important overall finding is that pulse modulation and spacer protection play complementary roles. Pulse modulation alone can substantially reduce rectal wall thermal damage when no spacer is present, whereas spacer insertion provides a dominant reduction in conductive heat transmission. When both strategies are combined, rectal wall safety is improved further while tumor damage remains close to the therapeutic threshold. These results indicate that multi-pulse laser delivery, particularly when used together with a clinically relevant HA spacer thickness, offers an effective strategy for preserving tumor ablation performance while minimizing collateral thermal injury to the rectal

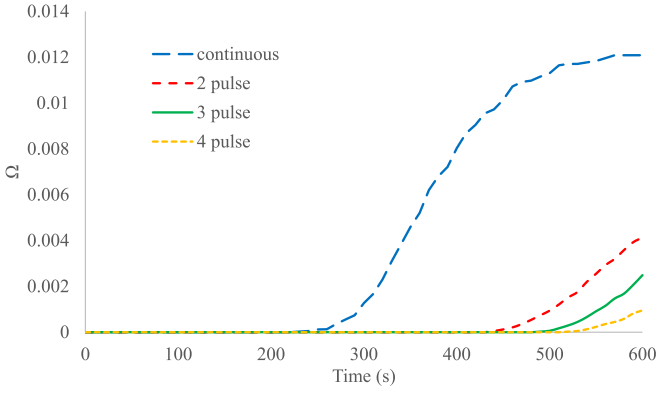

Fig. 11. Temporal evolution of the Arrhenius thermal damage parameter in the rectal wall under continuous, 2-pulse, 3-pulse, and 4-pulse laser irradiation with a 4 mm HA spacer.

wall. The same general balance between adequate target damage and reduced off-target thermal loading has also been emphasized in prior studies of pulsed laser heating and spacer-assisted prostate ablation. [9,16, 17, 20]

4.5. Combined effect of pulse number and HA spacer thickness on maximum rectal wall temperature

Fig. 12 presents the combined effects of pulse number and HA spacer thickness on the maximum rectal wall temperature. Two clear trends can be observed. First, increasing the HA spacer thickness consistently reduces the maximum rectal wall temperature for all irradiation modes. Second, for any given spacer thickness, increasing the number of pulses further lowers the peak rectal wall temperature compared with continuous irradiation.

To better relate these temperature results to thermal injury risk, the critical temperature thresholds of 55 °C and 60 °C are also indicated in Fig. 12. In general, temperatures around 55 °C are associated with the onset of irreversible thermal injury when sustained for a sufficient duration, whereas temperatures near 60 °C correspond to more rapid coagulative damage. These thresholds provide a practical reference for assessing whether the predicted rectal wall temperature remains within a safer range under different pulse configurations and spacer thicknesses. In the absence of an HA spacer 0 mm, the maximum rectal wall temperature is highest under continuous irradiation, indicating the most severe thermal exposure to the rectum. Under this condition, pulse modulation alone provides a substantial thermal benefit. Specifically, the maximum rectal wall temperature decreases by approximately 10.2%, 15.7%, and 20.4% for the 2-pulse, 3-pulse, and 4-pulse modes, respectively, relative to continuous irradiation. This result demonstrates that, even without a protective spacer, temporal redistribution of laser energy can significantly suppress excessive heat accumulation in the rectal wall. As the HA spacer thickness increases from 0 to 2 mm, a pronounced reduction in peak rectal wall temperature is observed for all irradiation modes. This indicates that even a relatively thin spacer provides an effective thermal barrier by increasing the prostate–rectum separation distance and reducing conductive heat transfer from the laser-heated prostate region toward the rectal wall [9,10]. With further increases in spacer thickness from 3 to 5 mm, the maximum rectal wall temperature continues to decrease, but the rate of reduction becomes progressively smaller. This behavior suggests a diminishing-return effect, whereby once the spacer has sufficiently weakened conductive heat transport, additional thickness provides only a limited further reduction in rectal thermal loading.

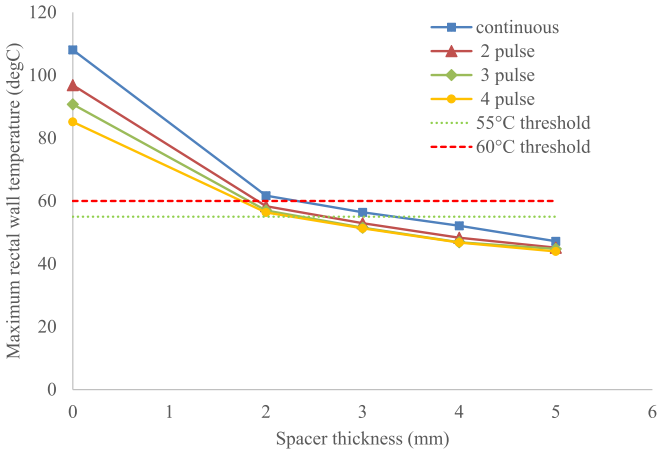

Fig. 12. Maximum rectal wall temperature as a function of HA spacer thickness for continuous and multi-pulse laser irradiation modes. The horizontal dashed lines indicate critical temperature thresholds associated with the onset of irreversible thermal injury (55 °C) and more rapid coagulative damage (60 °C).

The reduction in maximum rectal wall temperature results from the combined action of spatial and temporal protection. Spatially, the HA spacer acts as a low-conductivity intermediate layer and increases the distance between the heat source region and the rectal wall, thereby attenuating heat conduction across the multilayer domain [9,10]. Temporally, dividing the same total laser-on time into multiple pulses introduces OFF intervals that allow partial thermal relaxation before the next heating cycle begins. As a consequence, the cumulative thermal build-up in the rectal wall is reduced, leading to a lower peak temperature. Similar effects of intermittent laser delivery in limiting thermal accumulation have been reported in previous studies on repetitive and multiple-pulse laser heating in biological tissues [16,17].

An important observation from Fig. 12 is that the influence of pulse number is most pronounced when the spacer is absent or very thin, whereas the temperature difference among irradiation modes becomes smaller as the spacer thickness increases. This indicates that, at larger HA thicknesses, the dominant protective mechanism is the spatial thermal shielding provided by the spacer, while pulse modulation offers an additional but smaller reduction in peak rectal wall temperature. Nevertheless, the pulsed modes remain consistently lower than the continuous mode across the entire range of spacer thicknesses considered, confirming that pulse modulation and spacer insertion play complementary roles in rectal thermal protection.

Overall, these results show that both increasing HA spacer thickness and increasing pulse number are effective strategies for reducing the maximum rectal wall temperature. In particular, multi-pulse irradiation becomes especially beneficial when spacer thickness is limited, whereas thicker HA spacers provide a stronger baseline thermal protection regardless of the irradiation mode. This combined behavior highlights the potential of integrating temporal laser control with spacer-assisted thermal shielding to improve treatment safety in prostate laser therapy.

4.6. Combined effect of pulse number and HA spacer thickness on rectal wall thermal damage

Fig. 13 presents the combined effects of pulse number and HA spacer thickness on rectal wall thermal damage. Two major trends are evident. First, rectal wall thermal damage decreases markedly as the HA spacer thickness increases. Second, for any given spacer thickness, multi-pulse irradiation consistently results in lower rectal wall damage than continuous irradiation. These results indicate that both spatial separation and temporal modulation contribute to reducing collateral thermal injury during prostate laser therapy.

In the absence of an HA spacer 0 mm, continuous irradiation produces the highest rectal wall thermal damage, indicating the most severe collateral injury. Under this condition, the thermal damage of the rectal wall decreases by approximately 16.9%, 25.4%, and 26.6% for the 2-pulse, 3-pulse, and 4-pulse modes, respectively, relative to continuous

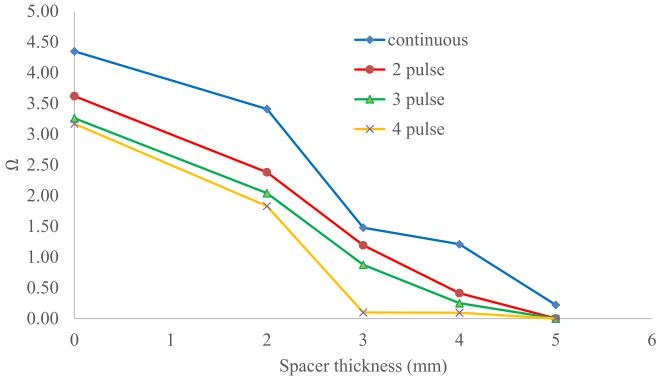

Fig. 13. Combined effects of pulse number and HA spacer thickness on rectal wall thermal damage under continuous and multi-pulse laser irradiation.

irradiation. This demonstrates that pulse modulation alone can substantially reduce rectal wall injury even when no protective spacer is used. The reduction arises because redistribution of the same total laser-on time into shorter pulses introduces cooling intervals, which interrupt continuous heat accumulation and lower the effective thermal dose delivered to the rectal wall [16,17].

As the HA spacer thickness increases from 0 to 2 mm, rectal wall thermal damage decreases sharply for all irradiation modes. This rapid reduction indicates that even a relatively thin spacer can significantly weaken conductive heat transfer from the laser-heated prostate region toward the rectum by increasing the prostate–rectum separation distance and introducing a low-conductivity thermal barrier [9,10]. When the spacer thickness is further increased from 3 to 5 mm, the damage continues to decline and approaches negligible levels, especially in the multi-pulse cases. In particular, the 4-pulse mode reduces rectal wall damage to nearly zero at a spacer thickness of 3 mm, whereas the continuous mode still predicts noticeable thermal injury at the same thickness. At 5 mm spacer thickness, rectal wall thermal damage becomes minimal for all irradiation modes.

From a physical perspective, this behavior reflects the strong temperature sensitivity of the Arrhenius damage integral. Because thermal damage depends exponentially on temperature, even moderate reductions in rectal wall temperature can lead to substantial decreases in the accumulated damage parameter. Therefore, the combined reduction in peak temperature and thermal residence time produced by spacer insertion and pulse modulation results in a disproportionately large decrease in rectal wall thermal damage. Similar findings have been reported in previous studies, where hydrogel spacers reduced rectal thermal exposure in prostate laser ablation [9,10], while repetitive or multiple-pulse laser delivery mitigated thermal accumulation and collateral injury in biological tissues [16,17]. An important observation from Fig. 12 is that pulse modulation is most beneficial when spacer thickness is absent or limited, whereas the influence of pulse number becomes less pronounced as the spacer thickness increases. This suggests that, at larger HA thicknesses, spatial thermal shielding becomes the dominant protective mechanism, while temporal modulation provides an additional but smaller improvement. Nevertheless, the pulsed modes remain consistently below the continuous mode over the entire range of spacer thicknesses considered, confirming that pulse modulation and spacer insertion play complementary roles in rectal wall protection.

4.7. Overall implications for treatment optimization

The present results indicate that treatment safety in prostate laser therapy can be improved through the combined optimization of pulse modulation and HA spacer thickness. In all simulated cases, increasing the number of pulses reduced rectal wall temperature and thermal damage, while increasing spacer thickness provided additional protection by suppressing conductive heat transfer toward the rectum. Importantly, the Arrhenius damage parameter in the tumor remained close to the ablative threshold in all irradiation modes, indicating that improved rectal protection was achieved without compromising tumor ablation efficacy. This balance between effective target destruction and minimization of collateral injury is central to treatment planning in laser-based prostate therapy, as also emphasized in recent optimization-oriented studies [13,14]. In the absence of a spacer, pulse modulation alone produced a clear protective effect. At 0 mm spacer thickness, the maximum rectal wall temperature decreased by approximately 10.2%, 15.7%, and 20.4% for the 2-pulse, 3-pulse, and 4-pulse modes, respectively, compared with continuous irradiation, while the corresponding rectal wall thermal damage decreased by approximately 16.9%, 25.4%, and 26.6%. These trends confirm that temporal redistribution of laser energy can effectively suppress heat accumulation and collateral thermal injury, consistent with previous studies on repetitive and multiple-pulse laser heating in biological tissues [16,17]. Spacer insertion further enhanced rectal protection. Increasing HA thickness from 0 to 2 mm produced the most pronounced reduction in both maximum rectal wall temperature and thermal damage, whereas further increases from 3 to 5 mm yielded smaller additional benefits, indicating a diminishing-return behavior once sufficient thermal separation had been achieved. This behavior is also consistent with clinical spacer literature, where the objective is to achieve sufficient prostate–rectum separation to reduce rectal exposure rather than to maximize spacing indefinitely. Reported clinical separations with hydrogel or HA-based spacers are often several millimeters to around 1 cm, but the incremental benefit of further separation may diminish once adequate protection is achieved. Accordingly, the present value of 3–4 mm should be interpreted as a model-based optimum for laser therapy under the investigated conditions, rather than a direct substitute for clinically reported spacing targets [26,27].

In addition, the use of the GDPL bioheat model strengthens the physical interpretation of these results because it accounts for phase-lag effects and non-Fourier heat transfer behavior under rapid laser heating conditions more realistically than classical bioheat formulations [11,13]. This makes the present framework suitable for evaluating the coupled roles of temporal energy delivery and spatial thermal shielding in prostate laser therapy. From a clinical implementation perspective, the proposed multi-pulse strategy appears feasible because focal laser ablation systems already support programmable energy delivery and real-time thermal monitoring [28]. Thus, multi-pulse irradiation may be incorporated as a temporal modulation protocol within existing treatment workflows to reduce rectal heating while preserving ablative efficacy. Nevertheless, direct clinical translation still requires further validation under patient-specific anatomical conditions and more realistic treatment settings, particularly in view of the simplifying assumptions adopted in the present model.

4.8. Comparison with previous numerical and clinical studies

Although the primary validation of the model was performed against published transient temperature histories, the predicted rectal protection trends were also compared qualitatively with previous numerical and clinical studies relevant to spacer-assisted prostate therapy. Since many published studies report rectal protection using clinical sparing metrics rather than Arrhenius-based thermal damage, these studies were used here as external comparative evidence rather than for direct one-to-one validation. Nevertheless, they consistently support the same general trend observed in this study, namely that increasing prostate–rectum separation improves rectal protection. A comparative summary of the present study and the relevant previous studies is provided in Table 3. In the present simulations, increasing HA spacer thickness reduced both the maximum rectal wall temperature and the associated thermal damage. This trend is qualitatively consistent with the numerical study of Namakshenas and Mojra (2021) [9], who reported reduced collateral rectal heating with PEG hydrogel spacer insertion during focal laser ablation, and with clinical spacer studies showing that greater prostate–rectum separation improves rectal sparing. Song et al. (2013) [29] reported successful creation of at least 7.5 mm separation in most patients with corresponding rectal dose reduction, while Narukawa et al. (2023) [25] and Björeland et al. (2023) [27] further showed that HA or PEG-based spacers significantly reduced rectal dose metrics in clinical practice. Previous pulse-laser studies also support the present interpretation that temporal modulation can alter transient heat accumulation and thermal damage behavior. Dutta and Kundu (2022) [30] showed that pulse-laser heating can better limit thermal injury to healthy tissue. Similarly, Wang et al. (2023) [31] demonstrated that pulse-laser irradiation significantly influences both thermal response and thermal damage behavior in biological tissue within a GDPL-based bioheat framework. Although these studies did not examine spacer-assisted multi-pulse delivery in the same framework as the present work, they strengthen the physical basis for the present finding that multi-pulse laser delivery can reduce rectal thermal loading while

Table 3
Comparative summary of the present study and previous spacer- and pulse-related studies relevant to rectal protection in prostate therapy.

	Spacer type / irradiation mode	Main finding relevant to the present study
Present study	HA spacer + continuous / multi-pulse laser	Increasing HA spacer thickness and pulse number reduced maximum rectal wall temperature and thermal damage, with a model-based optimum around 3–4 mm.
Namakshenas and Mojra (2021) [9]	PEG hydrogel spacer	Numerical analysis showed that spacer insertion reduced collateral rectal heating during focal laser ablation of a prostate peripheral zone tumor.
Song et al. (2013) [29]	PEG hydrogel spacer	Clinical results showed that increasing prostate–rectum separation reduced rectal exposure during prostate radiotherapy.
Björeland et al. (2023) [27]	HA spacer	HA spacer provided clinically meaningful rectal sparing and reduced high-dose rectal exposure.
Narukawa et al. (2023) [25]	PEG hydrogel spacer	Greater spacer separation was associated with lower rectal dose metrics, confirming the benefit of adequate spacing.
Dutta and Kundu (2022) [30]	Pulse-laser heating	Pulse-laser heating was reported to better limit thermally induced damage in healthy tissue.
Wang et al. (2023) [31]	Pulse-laser irradiation / GDPL-based bioheat model	Pulse-laser irradiation significantly influenced thermal response and thermal damage behavior in a GDPL-based bioheat framework with temperature-dependent properties.

maintaining tumor damage near the ablative threshold.

Overall, the present predictions are consistent with two complementary lines of previous evidence: spacer-related studies showing that increased prostate–rectum separation improves rectal protection, and pulse-related studies showing that temporal modulation of laser delivery modifies thermal response and damage behavior. Although the reported outcome measures differ across studies, the overall agreement in trend provides additional support for the credibility of the present numerical framework.

4.9. Limitations of the present model

Despite these promising findings, the present model has several limitations. The tissue layers were assumed to be homogeneous and isotropic, while real prostate and rectal tissues are anatomically heterogeneous and may exhibit anisotropic thermal behavior. In addition, patient-specific anatomy and irregular tumor geometry were not considered, and thermo-mechanical deformation, tissue shrinkage, and spacer displacement during heating were neglected. Therefore, the present findings should be interpreted as generalized trends rather than direct patient-specific predictions. Nevertheless, the model provides a useful framework for systematically examining the coupled effects of pulse modulation and HA spacer thickness on rectal wall thermal protection. Future studies should incorporate patient-specific geometry, heterogeneous tissue properties, and thermo-mechanical coupling to improve clinical realism.

5. Conclusion

A numerical study was conducted to investigate the coupled effects of laser irradiation mode and hyaluronic acid (HA) spacer thickness on rectal wall thermal protection during prostate laser therapy. A two-dimensional axisymmetric five-layer model, consisting of the rectal wall, HA spacer, the fat layer, prostate gland, and tumor, was simulated using the generalized dual-phase-lag (GDPL) bioheat model, while thermal damage was evaluated through the Arrhenius integral. Continuous, 2-pulse, 3-pulse, and 4-pulse irradiation modes were compared for spacer thicknesses ranging from 0 to 5 mm.

The results showed that both pulse modulation and HA spacer insertion significantly reduced the maximum rectal wall temperature and thermal damage. Without a spacer, multi-pulse irradiation reduced rectal wall temperature by up to 20.4% and thermal damage by up to 26.6% relative to continuous irradiation. Increasing spacer thickness provided further protection, with the most significant improvement observed between 0 and 2 mm, while additional benefit became less pronounced beyond 3–4 mm. Importantly, effective tumor ablation was maintained in all irradiation modes, with the tumor damage parameter remaining close to the therapeutic threshold.

Overall, the findings indicate that combining multi-pulse laser delivery with HA spacer protection can improve treatment safety without compromising ablation efficacy. In particular, multi-pulse irradiation is most beneficial when spacer thickness is limited, whereas an HA thickness of approximately 3–4 mm appears sufficient to provide substantial rectal thermal protection.

Nomenclatures

A	Frequency factor in the Arrhenius damage model (s^{-1})
a_h	Capillary surface area per unit tissue volume (m^{-1})
c_b	Specific heat capacity of blood (J/kg·K)
c_t	Specific heat capacity of tissue (J/kg·K)
C_{tb}	Ratio of tissue-to-blood specific heat capacity (−)
E_a	Activation energy in the Arrhenius damage model (J/mol)
g	Anisotropy factor (−)
h	Convective heat transfer coefficient at the outer rectal wall surface ($W/m^2·K$)
h_b	Convective heat transfer coefficient at the blood–tissue interface ($W/m^2·K$)
H	Heaviside step function (−)
k	Thermal conductivity (W/m·K)
k_b	Thermal conductivity of blood (W/m·K)
k_t	Thermal conductivity of tissue (W/m·K)
k_{eff}	Effective thermal conductivity (W/m·K)
k_{tb}	Ratio of tissue-to-blood thermal conductivity (−)
N	Number of pulses (−)
n	Outward unit normal vector (−)
Ω	Arrhenius thermal damage integral (−)
P	Laser power (W)
$Q_0(r,z)$	Spatially distributed laser heat source term (W/m^3)
$Q_{laser}(r,z,t)$	Volumetric laser heat generation term (W/m^3)
Q_{mb}	Metabolic heat generation in the blood phase (W/m^3)
Q_{mt}	Metabolic heat generation in the tissue phase (W/m^3)
r	Radial coordinate (m)
R	Universal gas constant (J/mol·K)
r_f	Optical fiber radius (m)
$S(t)$	Temporal modulation function representing the irradiation pattern (−)
t	Time (s)
t_n^{on}	Starting time of the n-th pulse (s)
t_n^{off}	Ending time of the n-th pulse (s)
T	Temperature (K)
T_b	Blood temperature (K)
T_t	Tissue temperature (K)
T_∞	Ambient temperature for convective boundary condition (K)
V	Blood velocity vector (m/s)
w	Blood perfusion rate (s^{-1})
z	Axial coordinate (m)
α	Absorption coefficient (m^{-1})
α_s	Scattering coefficient (m^{-1})

α_{eff}	Effective attenuation coefficient (m^{-1})
$\alpha_{th,eff}$	Effective thermal diffusivity (m^2/s)
ε	Porosity (−)
ρ	Density (kg/m^3)
ρ_b	Density of blood (kg/m^3)
ρ_t	Density of tissue (kg/m^3)
$(\rho_c)_{eff}$	Effective volumetric heat capacity ($J/m^3{\cdot}K$)
σ	Standard deviation of Gaussian beam distribution (m)
τ_q	Phase-lag time associated with heat flux (s)
τ_t	Phase-lag time associated with temperature gradient (s)

Subscript

b	blood phase
t	tissue phase
eff	effective property
laser	laser source term
mb	metabolic heat generation in the blood phase
mt	metabolic heat generation in the tissue phase
tb	tissue-to-blood ratio
f	optical fiber
∞	ambient or far-field condition
n	pulse number
u	upper side of an interface
d	lower side of an interface

CRediT authorship contribution statement

Phanuwat Boontatao: Writing – review & editing, Writing – original draft, Validation, Methodology. **Nattadon Pannucharoenwong:** Writing – review & editing, Writing – original draft, Validation, Methodology, Funding acquisition, Conceptualization. **Phadungsak Rattanadecho:** Validation. **Piyawat sermlao:** Validation. **Suphasit Panvichien:** Validation.

Declaration of competing interest

There is no conflict of interest.

Acknowledgements

This work was supported by the Thailand Science Research and Innovation Fundamental Fund fiscal year 2026 (Contract No. TUFF56/2569), Graduate Studies Faculty of Engineering, Thammasat School of Engineering (2023-2026), Thammasat University Thailand and this study was supported by Thammasat University Research Fund, Contract No TUFT 35/2567. The authors also wish to thank the Department of Mechanical and Industrial Engineering, Rajabhat Sakon Nakhon University, for its institutional support. The authors are likewise sincerely grateful to Asst. Prof. Dr. Teeravut Tubtawee, M.D., Department of Radiology, Faculty of Medicine, Prince of Songkla University, for his helpful advice and valuable contributions to this research. The authors further express their heartfelt thanks to all those who, in various ways, provided continuous encouragement, constructive suggestions, and support during the course of this study.

Data availability

Data will be made available on request.

References

[1] H. Sung, J. Ferlay, R.L. Siegel, M. Laversanne, I. Soerjomataram, A. Jemal, F. Bray, Global cancer statistics 2020: GLOBOCAN estimates of incidence and mortality worldwide for 36 cancers in 185 countries, CA Cancer J. Clin. 71 (3) (2021) 209–249.

[2] J.L. Mohler, E.S. Antonarakis, A.J. Armstrong, A.V. D'Amico, B.J. Davis, T. Dorff, J. A. Eastham, C.A. Enke, T.A. Farrington, C.S. Higano, E.M. Horwitz, M. Hurwitz, J. E. Ippolito, C.J. Kane, M.R. Kuettel, J.M. Lang, J. McKenney, G. Netto, D.F. Penson, E.R. Plimack, J.M. Pow-Sang, T.J. Pugh, S. Richey, M. Roach III, S. Rosenfeld, E. Schaeffer, A. Shabsigh, E.J. Small, D.E. Spratt, S. Srinivas, J. Tward, D.A. Shead, D. Freedman-Cass, NCCN clinical practice guidelines in oncology: prostate cancer, version 2.2019, J. Natl. Compr. Cancer Netw. 17 (5) (2019) 479–505.

[3] C. Parker, E. Castro, K. Fizazi, A. Heidenreich, P. Ost, G. Procopio, B. Tombal, S. Gillessen, Prostate cancer: ESMO clinical practice guidelines for diagnosis, treatment and follow-up, Ann. Oncol. 31 (9) (2020) 1119–1134.

[4] P. Wust, B. Hildebrandt, G. Sreenivasa, B. Rau, J. Gellermann, H. Riess, P. M. Schlag, Hyperthermia in combined treatment of cancer, Lancet Oncol. 3 (8) (2002) 487–497.

[5] N.R. Datta, S.G. Ordóñez, U.S. Gaipl, M.M. Paulides, J. Crezee, J. Gellermann, S. Bodis, Local hyperthermia combined with radiotherapy and/or chemotherapy: recent advances and promises for the future, Cancer Treat. Rev. 41 (9) (2015) 742–753.

[6] N. Mariados, J. Sylvester, D. Shah, L. Karsh, R. Hudes, D. Beyer, J. Michalski, Hydrogel spacer prospective multicenter randomized controlled pivotal trial: Dosimetric and clinical effects of perirectal spacer application in men undergoing prostate image guided intensity modulated radiation therapy, Int. J. Radiat. Oncol. Biol. Phys. 92 (5) (2015) 971–977.

[7] M. Pinkawa, V. Berneking, M. Schlenter, B. Krenkel, M.J. Eble, Quality of life after radiation therapy for prostate cancer with a hydrogel spacer: 5-year results, Int. J. Radiat. Oncol. Biol. Phys. 99 (2) (2017) 374–377.

[8] P.J. Prada, J. Fernández, A.A. Martínez, A. de la Rúa, J.M. Gonzalez, J. M. Fernández, G. Juan, Transperineal injection of hyaluronic acid in anterior perirectal fat to decrease rectal toxicity from radiation delivered with intensity-modulated brachytherapy or EBRT for prostate cancer patients, Int. J. Radiat. Oncol. Biol. Phys. 69 (1) (2007) 95–102.

[9] P. Namakshenas, A. Mojra, Optimization of polyethylene glycol-based hydrogel rectal spacer for focal laser ablation of prostate peripheral zone tumor, Phys. Med. 89 (2021) 104–113.

[10] P. Boontatao, N. Pannucharoenwong, P. Sermlao, S. Panvichien, Generalized dual-phase-lag modeling of rectal wall thermal protection in prostate laser therapy using hyaluronic acid, collagen, and balloon spacers, Int. J. Heat Mass Transf. 253 (2025) 127570.

[11] Y. Zhang, Generalized dual-phase lag bio-heat equations based on nonequilibrium heat transfer in living biological tissues, Int. J. Heat Mass Transf. 52 (21−22) (2009) 4829–4834.

[12] P. Kumar, D. Kumar, K.N. Rai, Numerical simulation of dual-phase-lag bioheat transfer model during thermal therapy, Math. Biosci. 281 (2016) 82–91.

[13] A. Andreozzi, L. Brunese, M. Iasiello, C. Tucci, G.P. Vanoli, Laser ablation for prostate tumors: analysis of different bioheat transfer models, Int. J. Therm. Sci. 217 (2025) 110026.

[14] G. Adabbo, A. Andreozzi, M. Iasiello, G. Napoli, G.P. Vanoli, Multi-objective optimization framework to plan laser ablation procedure for prostate tumors through a genetic algorithm, Comput. Methods Prog. Biomed. 267 (2025) 108827.

[15] H. Elkhalil, A. Alshare, G. Shafirstein, J. Bischof, A three-dimensional transient computational study of 532-nm laser thermal ablation in a geometrical model representing prostate tissue, Int. J. Hyperth. 35 (1) (2018) 568–577, https://doi.org/10.1080/02656736.2018.1512162.

[16] E. Jawo, M. Hassan, M.M.A. Almazah, Bio-thermal non-equilibrium dynamics and thermal damage in biological tissues induced by multiple time pulse-laser irradiations, Case Stud. Therm. Eng. 61 (2024) 104989.

[17] W. Preechaphonkul, V. Mongkol, P. Promoppatum, V. Srimaneepong, Comparative analysis of repetitive pulsed and continuous laser heating in multi-layered skin: bioheat vs. dual-phase lag model perspective, Int. J. Thermofluids 29 (2025) 101371.

[18] P. Boontatao, N. Pannuchareonwong, D. Nuasling, T. Chabuanoi, P. Rattanadecho, T. Tubtawee, S. Panvichien, Simulation of thermal effects on rectal wall during laser treatment of prostate cancer using hyaluronic acid and polyethylene glycol (PEG) spacers: a generalized dual-phase-lag (GDPL) bioheat approach, Eng. Sci. 33 (2025) 1308.

[19] M. Marin, A. Hobiny, I. Abbas, Finite element analysis of nonlinear bioheat model in skin tissue due to external thermal sources, Mathematics 9 (13) (2021) 1459.

[20] Y. Zhang, M. Liu, Y. Wang, Z. Wang, W. Zheng, Numerical simulation of heat transfer properties of skin tissue acted on repetitive laser irradiation, Int. Commun. Heat Mass Transf. 159 (2024) 108089.

[21] A. Andreozzi, L. Brunese, M. Iasiello, C. Tucci, G.P. Vanoli, A new thermal damage-controlled protocol for thermal ablation modeled with modified porous media-based bioheat equation with variable porosity, Processes 10 (2) (2022) 236.

[22] J. Saemathong, N. Pannucharoenwong, V. Mongkol, S. Vongpradubchai, P. Rattanadecho, Analyzing two laser thermal energy calculation equations: a comparison of Beer-Lambert's law and light transport equation, Eng. Sci. 24 (2023) 912, https://doi.org/10.30919/es912.

[23] X. Wu, K. Zhang, Y. Chen, R. Wang, L. Chen, A. Zhang, B. Hu, Theoretical and experimental study of dual-fiber laser ablation for prostate cancer, PLoS One 13 (10) (2018) e0206065.

[24] S. Zhang, C. Li, L. Cao, M.A.J. Moser, W. Zhang, Z. Qian, B. Zhang, Modeling and *ex vivo* experimental validation of liver tissue carbonization with laser ablation, Comput. Methods Prog. Biomed. 217 (2022) 106697.

[25] T. Narukawa, N. Aibe, M. Tsujimoto, T. Shiraishi, T. Kimoto, G. Suzuki, O. Ukimura, Increasing rectum–prostate distance using a hydrogel spacer to reduce radiation exposure during proton beam therapy for prostate cancer, Sci. Rep. 13 (2023) 18319.

[26] J. Yeh, B. Lehrich, C. Tran, A. Mesa, R. Baghdassarian, J. Yoshida, K. Tokita, Polyethylene glycol hydrogel rectal spacer implantation in patients with prostate cancer undergoing combination high-dose-rate brachytherapy and external beam radiotherapy, Brachytherapy 15 (3) (2016) 283–287.
[27] U. Björeland, K. Notstam, P. Fransson, K. Söderkvist, L. Beckman, J. Jonsson, C. Thellenberg Karlsson, Hyaluronic acid spacer in prostate cancer radiotherapy: dosimetric effects, spacer stability and long-term toxicity and PRO in a phase II study, Radiat. Oncol. 18 (1) (2023) 1.
[28] V. Iacovelli, M. Carilli, R. Bertolo, V. Forte, M. Vittori, B. Filippi, P. Bove, Transperineal laser ablation for focal therapy of localized prostate cancer: 12-month follow-up outcomes from a single prospective cohort study, Cancers 16 (15) (2024) 2620.
[29] D.Y. Song, K.K. Herfarth, M. Uhl, M.J. Eble, M. Pinkawa, B. van Triest, R. Kalisvaart, D.C. Weber, R. Miralbell, T.L. DeWeese, E.C. Ford, A multi-institutional clinical trial of rectal dose reduction via injected polyethylene-glycol hydrogel during IMRT for prostate cancer: analysis of dosimetric outcomes, Int. J. Radiat. Oncol. Biol. Phys. 87 (1) (2013) 81–87.
[30] J. Dutta, B. Kundu, Theoretical evaluation of bio-thermal response in human tissue subjected to pulse-laser induced hyperthermia therapy for cancer treatment, Int. J. Therm. Sci. 172 (2022) 107346.
[31] Y. Wang, X. Lu, W. Zheng, Z. Wang, Bio-thermal response and thermal damage in biological tissues with non-equilibrium effect and temperature-dependent properties induced by pulse-laser irradiation, J. Therm. Biol. 113 (2023) 103541.